PROCEEDINGS, 44th Workshop on Geothermal Reservoir Engineering
Stanford University, Stanford, California, February 11-13, 2019
SGP-TR-214

EGS Collab Experiment 1
Geomechanical and Hydrological Properties by Triaxial Direct Shear

Luke P. Frash[1], J. William Carey[1], Nathan J. Welch[1], and the EGS Collab Team[2]

[1]Los Alamos National Laboratory, PO Box 1663, Los Alamos, NM, 87545
[3]Multiple affiliations; team members listed in acknowledgements

lfrash@lanl.gov

Keywords: Permeability, Shear Strength, Hydroshear, Poorman's Schist, Tomography, Acoustic Velocity, Density, SURF.

ABSTRACT

We apply a triaxial direct-shear method to measure multiple geomechanical and hydrological properties of the Poorman's schist in the EGS Collab project's Experiment 1 (E1) test bed at the Sanford Underground Research Facility (SURF). Our method with integrated real-time x-ray imaging provides measurement of: 1) pre-shear natural fracture and matrix permeability, 2) natural fracture structure, 3) peak shear strength, 4) residual shear strength, 5) hydroshear critical pore pressures, 6) post-fracture permeability, 7) density, 8) acoustic velocity, 9) shear-dilation angles, and 10) aperture versus effective-stress correlations. The experiments use 25 mm diameter by 25 mm length right-regular cylinder core plugs. From these experiments, performed at actual site triaxial stress conditions, we have identified that natural foliation fractures containing graphite and/or aligned micas are the most likely features that could be hydroshear stimulated. We also find that the rock matrix permeability is very low, at less than 10 nD, which is less than previously expected. Hydroshear was successful after mechanically shearing the specimens but was not successful for bonded intact natural fractures or matrix rock.

1. INTRODUCTION

Developing enhanced geothermal systems (EGS) for energy production depends on engineering hydraulically conductive flow paths through hot geothermal reservoirs that may otherwise be uneconomic (Tester et al., 2006). Hydraulic shearing (hydroshearing) and hydraulic fracturing (fracking) offer two key well stimulation methods for increasing the hydraulic conductivity (i.e., permeability) of hot geothermal resources (McClure and Horne, 2014). Hydroshearing accomplishes permeability enhancement by increasing natural fracture connectivity and shear-dilating natural fractures. Fracking accomplishes the same with the addition of tensile fracture opening via injection at higher pressures and flow rates. Both of these stimulation methods have been studied extensively and deployed successfully, but the complexity of natural rock requires measuring a multitude of site-specific mechanical and hydraulic properties in order to have any hope of predicting the success of stimulation and optimizing stimulation design.

The Enhanced Geothermal Systems Collab team (EGS Collab) is executing meso-scale (~10 m) hydraulic stimulation experiments at the Sanford Underground Research Facility (SURF), in Lead, South Dakota (Kneafsey et al., 2018). This effort is part of an initiative to validate numerical models for EGS resource development and to support forthcoming full-scale experiments at the Frontier Observatory for Research in Geothermal Energy (FORGE). Both of these projects are sponsored by U.S. Department of Energy — Geothermal Technologies Office. The EGS Collab experiments are located in crystalline rock at 4000 to 5000 ft depth to simulate these respective features of sites where EGS technology could be deployed. This study focuses on the EGS Collab Experiment 1 site for which rock core, wireline logs, geological characterization, and geophysical data are available.

One goal in the EGS Collab project is to perform fracking experiments and hydroshear experiments. Hydroshearing requires in-situ shear stress and natural fractures that are favorably oriented such that increasing pore pressure from injection can induce shear slip. Fracking requires injection at high-rates to overcome matrix and natural fracture leak-off and high-pressures to induce tensile fracturing in the rock. The pressures and rates of fluid injection required for hydroshearing can be much less than those required for fracking. Site-specific geomechanical and hydrological testing provides the information needed to predict the flow rates and pressures required for each method of stimulation. Characterization of the mechanical and hydraulic properties of natural fractures is useful for selecting favorable injection locations to encourage or avoid hydroshearing and for evaluating the likelihood of shear along natural fractures.

In this study, we present test results from geomechanical experiments conducted at Los Alamos National Laboratory (LANL). These tests primarily used a triaxial direct shear apparatus integrated with an X-ray imaging system. Acoustic velocities were measured for each core using a separate system prior to the triaxial direct shear testing. Results from these experiments provide: permeability, shear strength, hydroshear critical pressures, density, acoustic velocities, shear-dilation angles, and aperture versus effective-stress correlations. These measured parameters provide inputs to geomechanical and hydrological models and are useful for interpreting field results.

2. GEOLOGY SETTING

The site of the first set of stimulation experiments for EGS Collab is at SURF in Lead, South Dakota which is on the northern side of the Black Hills in Precambrian aged crystalline rock. Graphite, pyrite, calcite, sulfides, and quartz are all present in the Poorman's schist at significant heterogeneous and anisotropic concentrations. Experiment 1 for this project is located 1478 m (4850 ft) below the nominal ground surface in the Poorman's schist geologic unit. The overburden (vertical) stress at this site is estimated at 44 ±5 MPa and the

minimum principal stress was measured at 24 ±2.5 MPa from a set of vertical borehole minifrac tests (Oldenburg et al., 2016). The difference between the maximum and minimum in-situ stresses provides in-situ shear stress and is a requirement for hydroshearing. Rock core and well logs are available from vertical, north oriented sub-horizontal, and west oriented sub-horizontal boreholes from which a multitude of natural fractures with vertically dominated dip were identified (Ulrich et al., 2018). Two dominant sub-vertical joint sets exist at the site, one aligned with south-east strike and another aligned with south-west strike. For this study, core containing natural fractures were extracted from the E1-P well (production well) at depths of 28.3 m (93 ft) and 52.1 m (171 ft). The sampled natural fractures included calcite infilled veins (0 to 2 mm thick) and foliation fractures that may or may not have been induced by drilling. Geomechanical tests were conducted to measure the shear properties, hydraulic properties, and anisotropic acoustic properties of intact rock, the two sets of natural calcite infilled veins, and the foliation.

3. EXPERIMENT METHODS

Three separable methods were used to obtain the measurements presented in this study. First, the specimens were prepared so as to sample natural fractures and features of interest and to measure density. Second, compressive and shear wave velocities were measured using conventional tools. Third, triaxial direct-shear experiments were performed. Of these, the third step was the most complex with the inclusion of unconventional methods such as x-ray imaging and custom methods to analyze the resulting data.

3.1 Sample Preparation and Density Measurement

Rock specimens were prepared as precision right-regular cylinder core plugs (Figure 1) following ASTM D4543-08 (2008). Core plug dimensions were nominally 25.4 mm diameter and 25.4 mm length. Calcite infilled veins were strong enough to maintain integrity through preparation. The host core from which these core plugs were extracted was HQ size. Extreme care was taken to identify and sub-core natural fractures parallel to and along the diametric cross section of the cores so as to be suitable for mechanical and hydraulic characterization of each major in-situ fracture set. As shown, PS01-03 and PS01-06 were foliation parallel and therefore most likely belonging to the south-east striking in-situ joint set. PS01-01 was oriented perpendicular to this joint set to measure matrix properties. PS01-08 contains fractures from both the south-east and south-west joint sets with the larger vein being from the south-west joint set. Specimen saturation was room condition, without steps taken for drying or saturation, because porosity was low for this material. Density was directly measured for every specimen (9 total count) using calipers and a mass-balance.

Figure 1: Subset of the prepared Poorman's schist specimens having 25.4 mm nominal diameter and cored to position natural fractures parallel with the plane of direct shear for hydraulic and geomechanical characterization.

3.2 Acoustic Velocity Measurement

Acoustic compression wave (P-wave) and shear-wave (S-wave) velocity was measured parallel and perpendicular to the foliation using a GCTS ULT-200 system with 25.4 mm flat platens. This method uses unipolar pulse excitation of source piezo-electric crystals and passive monitoring and averaging of 8 waveforms recoded on receiver piezo-electric crystals. Arrival times in these signals were manually picked. Calibration for head-to-head arrival time and wave speed through a 25.4 mm diameter 63.5 mm long 6061-T6 aluminum specimen was used to improve the accuracy of the measurement. No differentiation between orthogonal S-wave orientations was possible with our setup (e.g., S1 and S2). Uncertainty in manually picked arrival times is included in the reported wave speed measurements. A thin layer of honey was used for acoustic couplant. Measurements were acquired along the axis of the cores and perpendicular to the axis of the cores. Normal stress for contact was provided by the weight of the acoustic platen because forces higher than this risked fracturing the specimen by indirect tension.

3.3 Triaxial Direct Shear Test and Associated Measurements

The latest generation (third) of the LANL triaxial direct-shear apparatus was used for geomechancial and hydrological characterization of the natural fractures and intact matrix of the Poorman's schist. This apparatus is integrated with x-ray imaging to obtain radiographs during shearing at elevated confining stresses (i.e., video) and to perform computed tomography to resolve fracture pore structure. As an unconventional apparatus, the methods used to calibrate, measure, and evaluate results are all custom and the descriptions of these methods to follow will be abbreviated for this document. For questions or clarifications, please contact the corresponding author.

3.3.1 Triaxial Direct Shear Apparatus

The triaxial-direct shear apparatus shown in Figure 2 provides radial confining stresses up to 35 MPa, axial compression of up to 240 kN, and temperature up to 100 °C via an aluminum body vessel that is transparent to x-rays and neutrons. This system was originally detailed by Carey et al. (2015a; 2015b; 2016) and modified by Frash et al. (2016a; 2017; 2018; 2019) to give the current setup shown. Confining fluid pressure is applied outside of the FEP sleeve to compress the specimen across its outer radius (σ'_c) and on half of each end of the specimen (F_c). Axial force through two opposing L-shaped hardened steel thrust collars (F_p) is used to generate direct-shear stress through the specimen. This thrust load induces stress concentrations at the corners of the collars (Figure 2b) which is advantageous for creating shear fractures that connect between these two corners and are therefore suitably aligned for hydraulic conductivity measurement (i.e., permeability). This direct-shear load path can also be aligned with natural fractures to measure their geomechanical properties more directly. The shear stress inside of the specimen is not uniform but it is predictable due to direct control and measurement of all the boundary conditions. Compared to conventional direct-shear tests (e.g., ASTM D5607), the confining stress in this system is triaxial, instead of uniaxial, and all six components of the stress tensor are controlled. Pore fluids are injected through a conduit on each end that permits flow through the fracture and onto both end faces of the specimens for intact permeability measurement. Rotation of the specimen due to asymmetric direct-shear loading is limited by the collar and piston assembly tolerances. Control of the hydraulics system for confining pressure, axial pressure (direct-shear), and pore fluids is provided by a system of six Teledyne Isco pumps and DIsco software (https://www.lanl.gov/projects/feynman-center/deploying-innovation/intellectual-property/software-tools/disco/index.php). Nitrogen is used as a confining fluid for improved x-ray transparency. Pore fluid is tap water with flow and pressure measured at the inlet and outlet.

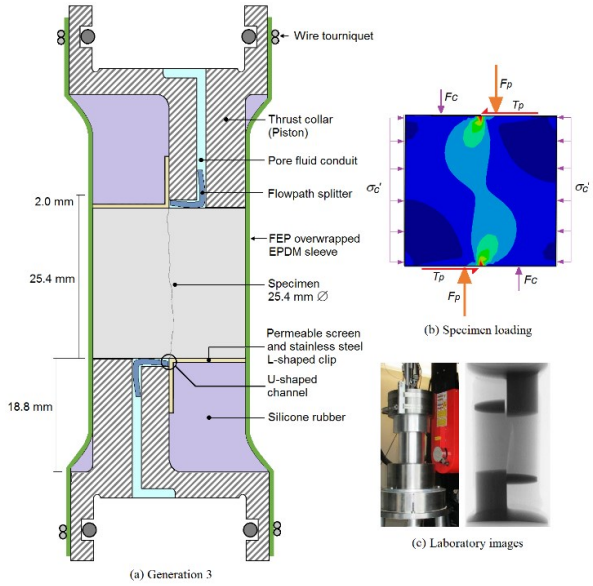

Figure 2: Triaxial direct-shear assembly. (a) The naturally fractured specimen is aligned parallel with the direct-shear plane imposed by two opposing and offset thrust collars. (b) Abaqus finite element modeling of shear stress distribution in the specimen. (c) The apparatus viewed in the x-ray cabinet and an x-ray image of a fractured specimen through the vessel.

3.3.2 In-Situ Stress Simulation

The triaxial direct-shear tests in this study included simulation of in-situ compression and shear stress conditions from the EGS Collab E1 test bed at an orientation suitable for shearing. As part of this, a benchtop gravity slant shear test was used to estimate a Mohr-Coulomb friction angle of 30° and a cohesion of 0 MPa for a separated natural foliation fracture in the HQ rock core. For the known in-situ maximum and minimum principal stresses at the E1 site of 44 MPa and 24 MPa, respectively, we use these interface shear properties in a Mohr-Coulomb analysis to predict that shear slip could occur on a natural fracture oriented at ~60° dip and south-east strike. The corresponding total normal stress at this slip condition is 29.0 MPa, the shear stress is 5.8 MPa, and the pore pressure is 13.9 MPa. By similar analysis, the maximum expected in-situ shear stress at the E1 site is ~10 MPa and the total normal stress on a slip-capable fracture can reasonably range from 26 to 32 MPa. Therefore, to simulate these slip conditions in the triaxial direct-shear apparatus we applied 29.0 MPa of total confining stress (σ_c), a nominal direct-shear stress of 9.0 MPa (τ_{DS}), and pore pressure ranging from 0 to 28 MPa as limited by the confining stress sleeve-seal. This analysis utilized the following common Mohr-Coulomb and Terzhaghi's effective stress relationships:

$$\sigma' = \sigma - p \tag{1}$$

$$\tau_n = \sigma'_n \tan(\varphi) + c \tag{2}$$

$$\sigma_n = \frac{\sigma_1+\sigma_3}{2} + \frac{\sigma_1-\sigma_3}{2}\cos(2\theta) \tag{3}$$

$$\tau_n = \frac{\sigma_1-\sigma_3}{2}\sin(2\theta) \tag{4}$$

Where, σ is total normal stress, τ is shear stress, (') denotes effective stress, p is fracture or pore pressure, (n) denotes stress on an oriented surface, θ is the angle from vertical (i.e., the maximum principal stress) to the normal of this oriented surface, φ is the interface friction angle of this surface, c is the cohesion strength of this surface, and (1) and (3) denote the maximum and minimum in-situ principal stresses respectively. Additional details on how this analysis is conducted can be found in any major geotechnical engineering textbook.

To best address the question of whether or not the natural fractures in the E1 test bed are prone to hydroshear stimulation, one can make use of the following relationship which is derived from Equations (1-4) to predict the minimum injection fluid pressure (P_{ic}) required to enable hydroshearing of an optimally oriented natural fracture. Less optimally oriented fractures will require higher injection pressure.

$$P_{ic} = 0.5(\sigma_1 + \sigma_3) + \frac{c}{tan(\varphi)} - 0.5(\sigma_1 - \sigma_3)/sin(\varphi) \quad (5)$$

This critical pressure for hydroshearing can also be verified in the triaxial direct-shear test by applying the associated oriented total normal and shear stresses prior to increasing the pore pressure and monitoring for shear displacement. For a related practical matter, it is not possible for the injection pressure to exceed the hydraulic fracturing breakdown pressure which has been measured at ~30 MPa for the E1 site, unless shock inducing methods are used (e.g., explosives; Frash et al., 2015). Normal stress is taken as positive for compression.

3.3.3 Test Procedure

For each triaxial direct-shear test the following protocol was applied (Figure 3):

1. Isotropic confining stress of 3.5 MPa is applied (no shear) and initial specimen permeability is measured. Inlet pore pressure is set at 1.5 MPa with a 1.0 mL/min flow rate limit. Outlet pressure is set at 0.5 MPa with a 2.0 mL/min limit.

2. Isotropic confining stress is increased to 29.0 MPa and 5 to 15 min of relaxation and saturation time is allowed. This provides an additional measurement of initial specimen permeability at in-situ stress conditions.

3. Direct-shear stress is increased to 9.0 MPa and hydroshearing is attempted by increasing the pore pressure to a maximum of 28.0 MPa. Inlet pore pressure is increased first with a 2.0 mL/min maximum flow rate. If the specimen is highly permeable, pore pressure increase is achieved by restricting the outlet flow rate. Furthermore, the shear displacement rate is limited to prevent excessive slip if hydroshear occurs. This step ends and pore pressure is reduced to the original values if slip occurs.

4. If hydroshear was unsuccessful, mechanical shearing is performed by increasing the direct-shear stress at a steady rate until shear slip is observed. Confining stress is maintained at 29.0 MPa.

5. A second attempt at hydroshearing is completed using the same procedure as before (step 3).

6. Additional mechanical shear or hydroshear steps are conducted at varying effective confining stresses to parameterize the shear slip criteria for the fractured specimen and changes in other specimen properties (e.g., aperture) as a function of confining stress.

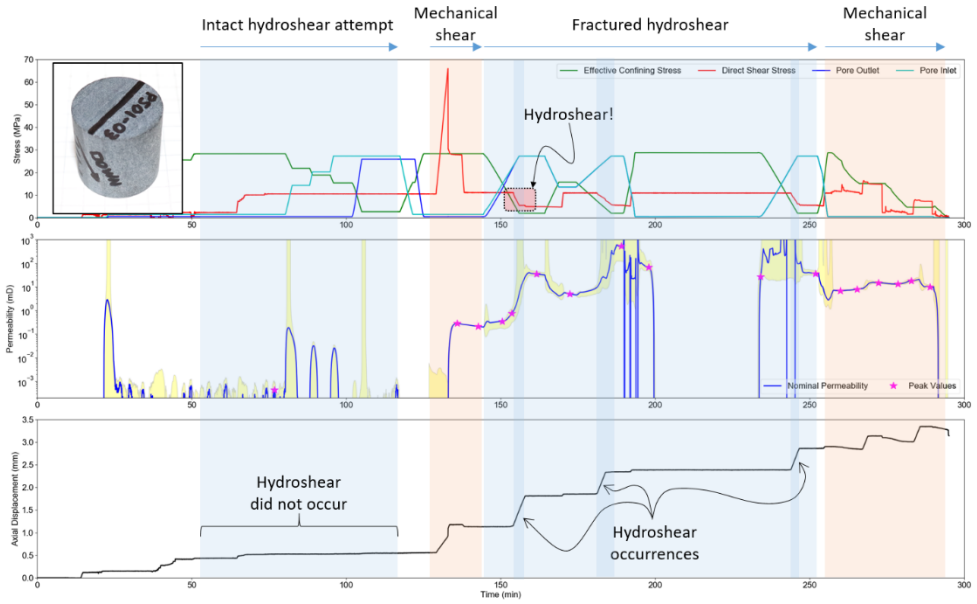

Figure 3: Typical test protocol with hydroshear simulation attempted before and after a mechanical shear event. Hydroshear is attempted by maintaining a nominal shear stress of 9.0 MPa at 29.0 MPa of total confining stress while raising the pore pressure up to a maximum of 28.0 MPa. Data from the PS01-03 specimen which was parallel to intact foliation is shown.

3.3.4 Geomechanical Strength Measurement

The mean direct-shear stress (τ_{DS}) applied to the specimen is estimated using the following relationship with reference to Figure 2:

$$\tau_{DS} = \frac{F_P - F_C}{DL} - \sigma_S \quad (6)$$

Where, D is the specimen diameter, L is the specimen length, and σ_S is a calibration value at 2.0 ±2.0 MPa from tests conducted on split specimens of greased Teflon. The respective end force values (F_P and F_C) are measured by calibrated pressure transducers. The end shear force (T_P) is emergent from static equilibrium and is in balance with the direct-shear force.

Intact matrix shear strength and bonded natural fracture shear strength are measured from the peak direct-shear stress required to fracture and first slip the specimen. Residual shear strength is measured from the direct-shear stress required to continue to displace the fractured specimen in shear. Generally, the intact strength should have higher friction angle and cohesion than the residual. Strength values obtained at different confining stress, whether induced by changing pore pressure or total confining stress, are used to estimate the Mohr-Coulomb parameters in Equation (2).

3.3.5 Aperture Measurements: Hydraulic, Dilatational, and Local

The aperture of a fracture can be viewed as the distribution of local void space, as the mean separation of adjacent fracture surfaces, and as the effective hydraulic opening which permits fluid flow. We estimate all three of these in triaxial direct-shear experiments using direct measurements of pore fluid flow (i.e., permeability) and physical aperture from x-ray imaging (Frash et al., 2019).

For the effective hydraulic opening (i.e., hydraulic aperture; b_h) we apply the inverse cubic law (Boussinesq, 1868; Witherspoon et al., 1980; Zimmerman and Bovarsson, 1996) for parallel plate flow to calibrated measurements of pressure drop across the specimen (ΔP), the specimen's length (L) and diameter (D), and the associated upstream and downstream flow rates (Q) with the assumption of room temperature water viscosity (μ) at 0.9 cP:

$$b_h = \sqrt[3]{\frac{12Q\mu L}{-\Delta P D}} \quad (7)$$

This is relatable to Darcy permeability (k) measurement for the whole core via the following relationships:

$$b_h = \sqrt[3]{3\pi D k} \quad (8)$$

$$k = \frac{Q\mu L}{1/4 \pi D^2 \Delta P} \quad (9)$$

We report both permeability and hydraulic aperture, using the value most relevant to its context. We find that hydraulic aperture is a useful means to represent fluid conductivity of a fracture because the value can be more directly scaled to fractures of different length and width and the value is not as sensitive to the cross-sectional geometry of the specimen.

For the mean and local separation of adjacent fractures, we use two x-ray imaging methods that are implemented through the triaxial direct-shear apparatus at elevated confining stress. First, we apply thresholded Sobel edge detection to radiographs that are acquired during shearing events to estimate the dilation of the specimen normal to the direction of shear. We refer to this value as dilatational aperture (b_d) and we are able to measure it rapidly at 0.5 Hz. Second, we compute the mean aperture over the length and width of the fracture using segmented computed-tomography reconstruction of the 3D fracture void space. We refer to this value as mean local aperture (b_l) and measure this more slowly at one reconstruction per 2 hr scan. Spatial distribution of fracture aperture (e.g., roughness, asperity contacts, and stranding) is also obtained from the computed tomography. There are many detailed steps to estimate b_d and b_l that include associated custom algorithms and user-picked thresholding values. In short, we present our best estimates of these respective values but also acknowledge that these estimates do have uncertainty arising from artifacts of the analysis methods used. In prior work (Frash et al., 2019), we found that the two mean mechanical aperture values (b_d and b_l) tend to closely agree for many brittle rock types, including shale, anhydrite, and dolomite, but the hydraulic aperture (b_h) tends to be much smaller by single to multiple orders of magnitude.

3.3.6 Aperture and Stress Relationships

To evaluate the functional relationship between aperture and stress, we employ the Barton-Bandis relationship for matched joints via the following (Barton et al., 1983):

$$b_d = b_{max} + A\Delta\sigma_n'/(1 - B\Delta\sigma_n') \quad (10)$$

$$A/B = b_{max} - b_{min} \quad (11)$$

$$\Delta b_d = b_{max} - b_d \quad (12)$$

Where, $\Delta\sigma'_n$ is change in the effective normal stress across a fracture and b_{max} and b_{min} are estimates of the fracture aperture at zero stress and infinite stress, respectively. Since this function is empirical, we choose to set b_{min} to 0.0 to signify full closure of the fracture at high stress and to avoid least-squares curve fits that predict non-physical values for b_{min}. It is important to note that the geometry of a fracture depends on the stress at which the fracture was formed (Frash et al., 2017; Frash et al., 2019), which is a separate effect.

4. MEASUREMENTS AND RESULTS

Ten specimens have been prepared to date, all of which were used to measure rock density. Acoustic velocity measurements were taken on every specimen but so-far analyzed for only two, PS01-01 ad PS01-03, to give values for wave speed through intact rock matrix perpendicular to and parallel to the foliation. Triaxial direct-shear tests were completed on the following four specimens: 1) PS01-03 — an intact foliation parallel specimen, 2) PS01-06 — an intact calcite infilled natural fracture parallel with foliation, 3) PS01-09 — an intact calcite infilled natural fracture specimen at an off-angle to the foliation, and 4) PS01-11 — a pre-fractured specimen from a weak foliation that separated during field drilling. Acoustic velocity measurements, density, and permeability are summarized in Table 1. Geomechanical measurements are summarized by Mohr-Coulomb type friction angle, cohesion, and critical injection pressure measurements in Table 2. These geomechanical values are also shown in Figure 4 within the context of a Mohr-Coulomb stress-circle slip analysis. X-ray image results are presented in Figures 5 through 7. Supporting data is available upon reasonable request to the author.

4.1 Density Uniformity, Acoustic Velocity Anisotropy, and Matrix versus Fracture Permeability

Density measurements were very consistent (±0.023 g/cm^3) with slightly lower densities measured for specimens containing larger natural fractures. Also, the density was slightly lower in the interval containing weak foliations at 52.1 m into E1-P. This lower density interval is suspected to associate with carbonate leaching by in-situ fluid flow because this interval did not react strongly to HCl even though most other intervals from this E1-P core did.

Table 1: Measured density, acoustic velocity, and permeability of the Poorman's schist.

Parameter	Value	Unit
ρ – Density	2.765 ±0.023*	g/cc
Vp – Parallel foliation	5750 ±100^{T01} or 5480 ±100^{A03}	m/s
Vs – Parallel foliation	4240 ±130^{T01} or 3190 ±130^{A03}	m/s
Vp – Perpendicular foliation	5400 ±140^{A01} or 3650 ±180^{T03}	m/s
Vs – Perpendicular foliation	3090 ±130^{A01} or 1260 ±200^{T03}	m/s
k – Intact matrix or bonded fracture	0.001 (max.)	mD
k – Infilled not parallel foliation	0.1 (1 to 0.001)	mD
k – Intact foliation	10.0 (100 to 1)	mD
k – Infilled and parallel foliation	0.10 (6 to 0.03)	mD
k – Pre-fractured weak foliation	0.008 (20 to 0.001)	mD

* Lower around calcite veins & 0.01 g/cc lower at 93 ft than 171 ft in E1-P
A Measurement along core axis
T Measurement transverse to core axis

Acoustic velocity measurements indicate strong anisotropy, especially for shear waves (V_s at 4240 m/s to 1260 m/s), with the higher velocities occurring parallel with the foliation. This result agrees with prior work from the kISMET project at SURF which used different measurement methods (Oldenburg, 2016). The reduced velocity perpendicular to foliation could indicate that the foliation is likely to dampen S-waves through micro-scale inelastic slip and that a uniform velocity model would not be ideal for future attempts at microseismic event source location. Heterogeneity in the rock structure is also evident by comparing the data for PS01-01 and PS01-03, which were obtained from 28.3 m and 52.1 m into E1-P, respectively. It is hoped that these values represent the extremes. Acoustic attenuation parameters were not measured for these specimens. Systemic errors arising when comparing measurements along the core axis versus transverse to this axis were not evaluated.

The triaxial direct-shear experiments indicate that the matrix permeability of the Poorman's schist matrix is likely to be no greater than 0.001 mD. This matrix permeability value was previously estimated at 1-2 orders magnitude larger in early modelling efforts. Also, the intact permeability of most of the natural fractures appears to be as low as the matrix. The largest increase to hydraulic permeability occurred when shearing an initially intact foliation (PS01-03) and the lowest increase occurred when shearing a pre-fractured foliation (PS01-11). A more broad distribution of slippery gouge material in the weaker pre-fractured foliation contributed to this apparent inconsistency. It is difficult, and perhaps even inappropriate, to attempt to draw many conclusions based on these measured permeabilities without also considering the associated aperture measurements from x-ray imaging. It is also important to note that permeability though a rough sheared fracture will strongly depend on the direction of fluid flow, presence generated transportable fines, geochemical and biological infilling, and the location of the fluid flow sources and sinks relative to local roughness distributions (Detwiler and Morris, 2014; Gentier et al., 1997; Frash et al., 2019). In other words, it is not surprising to see significant variability in fracture permeability measured using the triaxial direct-shear method and a similar or greater level of variability should be assumed for the field. Taking for example the E1 site, permeability variability through a hydraulic fracture stimulated interval has been observed through long term injections at constant pressures and constant flow rates.

4.2 Geomechanical Strengths and Hydroshear Potential

Measured geomechanical parameters from the four tested specimens are given in Table 2 and depicted in a Mohr-Coulomb slip analysis via Figure 4. These results indicate that hydroshear is possible in the E1 test bed with foliation parallel fractures being the most likely to slip in hydroshear. Fractures not parallel to the foliation appear unable to hydroshear because the required critical slip injection pressure exceeds 30 MPa, but there may be exceptions in the field. Hydroshear was successfully induced on foliation parallel specimens using the triaxial direct-shear apparatus at simulated in-situ stress conditions (PS01-03, PS01-06, and PS01-11). Of these, only the pre-fractured weak foliation specimen (PS01-11) was successfully hydrosheared before forcing mechanical shear via increasing the shear stress.

Table 2: Measured shear strength of matrix, small infilled fractures, and foliation in the Poorman's schist.

Feature	Friction angle (φ)	Cohesion (c)	Critical slip pressure (P_{ic})
Intact: Matrix or bonded fracture (PS01-03, 06, & 09)	59°	20 MPa	34 MPa
Residual: Infilled not parallel foliation (PS01-09)	48°	13 MPa	32 MPa
Residual: Intact strong foliation (PS01-03)	41°	4 MPa	23 MPa
Residual: Infilled parallel foliation (PS01-06)	36°	4 MPa	22 MPa
Residual: Pre-fractured weak foliation (PS01-11)	17°	2 MPa	6 MPa

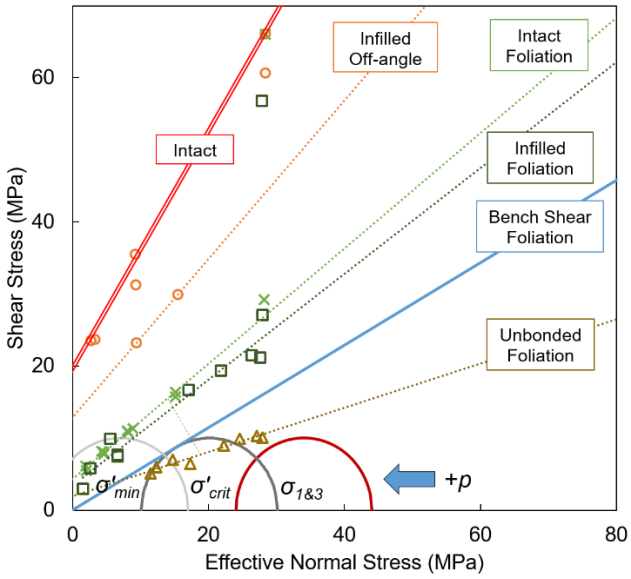

Figure 4: Measured triaxial direct-shear stresses in Mohr-Coulomb slip analysis. Of the tested samples, hydroshear was only successful on natural fractures parallel with foliation because they exhibited low strength. Mohr's stress circles are plotted for the in-situ total stress ($\sigma_{1\&3}$; rightmost), the predicted critical effective stress from bench shear testing (σ'_{crit}; center), and minimum effective stress at the hydraulic fracture limit (σ'_{min}; leftmost). These circles show that hydroshear could occur at injection pressures as low as 6 MPa for optimally oriented unbonded (i.e., pre-fractured) weak foliation fractures.

In the field, slip along any natural fracture will perturb the local stress state though complex fracture interactions and stress concentrations. We do not attempt to evaluate these spatial interaction effects in this document but it is important to recognize that these effects can cause localized slip along high strength natural fractures and also reduce shearing potential along any but the weakest fractures. In effect, the weakest fractures are likely to dominate hydroshear induced slip when they are present in the zone of injection. The weak foliation fractures (e.g., PS01-11 and PS01-06) generally coincide with the optimum orientation for shear at the E1 site with south-east strike and ~60° dip. Therefore, these fractures should make good targets for intentional hydroshear stimulation.

With regard to the natural fracture permeability, the intact permeability of most of the natural fractures appears to be as low as the matrix and the strength of these appear to be nearly as high as the intact matrix. Because of this, initiating hydroshear could be difficult or impossible unless injecting into un-bonded fractures or more permeable fractures than those tested here. Hydraulically conductive fractures are known to exist in the E1 test bed. Another indication from this data is that hydrofracking at pressures above 25 MPa is likely to open natural fractures by overcoming the tensile strength and this will subsequently enable hydroshearing by providing these now permeable natural fractures with the necessary fluid pressure for slip. If observing the dilation and shear across a fracture, this would predict tensile opening prior to shear slip.

Qualitative observation of the fractured specimens found significant gouge material formed in the pre-fractured foliation parallel specimen (PS01-11) and also some gouge in the other foliation parallel specimens (PS01-03 and PS01-06). This gouge material appeared to have a low friction graphitic structure that lubricated the fracture for slip but also blocked fluid flow by infilling the pore space. The weakest foliation was the PS01-11 specimen which was obtained from the E1-P well at 52.1 m (171 ft) from a segment of core that could be crumbled by hand. Crumbling the rock by hand was not possible on any other interval of the E1-P well.

4.3 X-ray Image Analysis for Mechanical Local and Dilatational Apertures

X-ray image data was obtained for PS01-06 and PS01-11, being the infilled foliation parallel fracture specimen and the pre-fractured weak foliation specimen, respectively. Analysis of this image data is still in progress. Figure 5 shows the distribution of segmented local aperture in the PS01-06 specimen. This specimen was successfully sheared along the natural foliation (central low-aperture area) with the exception of short opening fracture segments through the matrix rock (near to the ends of the specimen). The created fracture appeared to have little direct interaction with the pre-existing infilled natural fracture because the created shear fracture was visually interwoven with the infilled fracture rather than coincident. The pre-shear x-ray tomography did not show any significant contrast between the infilling fractures and the matrix despite the infilled fractured being larger than the 47 μm resolution of the scanner. This indicates that the infilled natural fracture has similar strength to the matrix and that the foliation dominates shear slip behavior.

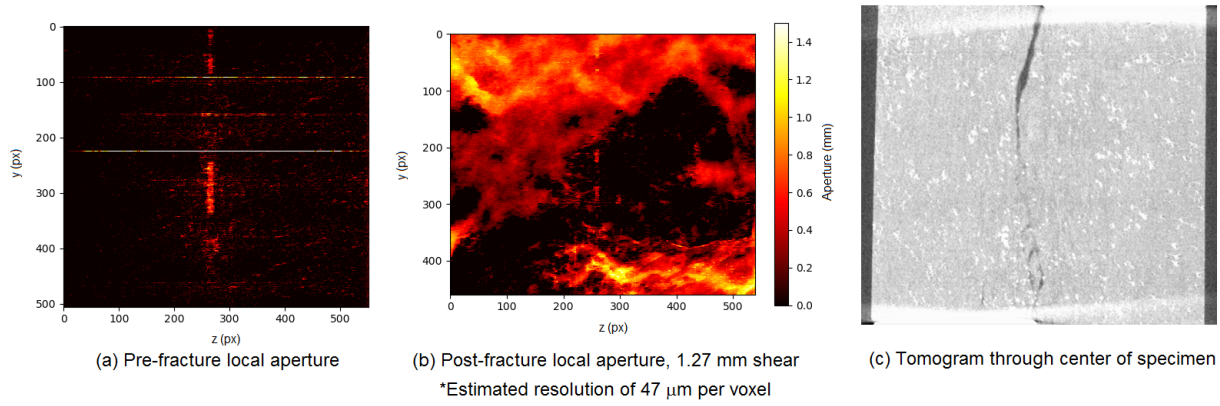

Figure 5: Local aperture distribution from segmented tomograms for PS01-06 — infilled foliation parallel natural fracture. (a) Total aperture projected onto the direct-shear plane prior to shearing. (b) Projected aperture after shearing. (c) A center cross-section showing the shape of the facture in the x-axis. The apparent S-shaped 'en echelon fracturelet' geometry is typical of the triaxial direct shear test for homogeneous intact specimens (Frash et al., 2019). This indicates that the pre-existing infilled fracture had little effect on created geometry.

The x-ray radiography enables comparison of the hydraulic aperture with the mechanical dilatational aperture and the general structure of the fracture (Figure 6). As is typical of rough shear fractures (Frash et al., 2019), the hydraulic aperture parallel to the direction of shearing was significantly smaller (~1.3 to 2.3 order magnitude) than the dilatational aperture. Recall that hydraulic conductivity has a cubic relationship to hydraulic aperture (Equation 8). The hydraulic conductivity perpendicular to the direction of shear is expected to be higher.

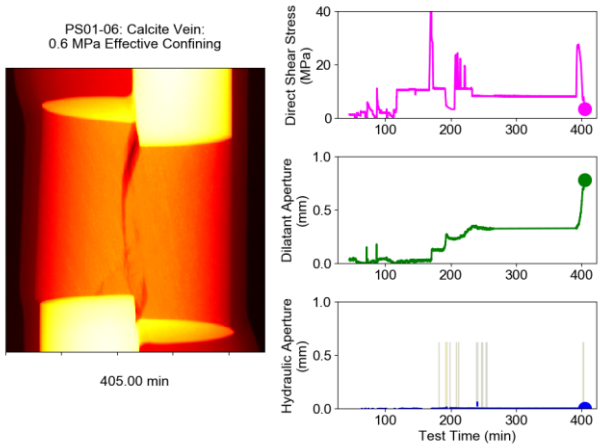

Figure 6: Correlated x-ray measured dilatational aperture and hydraulic aperture from PS01-06, the specimen containing a natural infilled foliation parallel fracture. Hydraulic aperture parallel to the direction of shearing is significantly less than the dilatant aperture by a factor of 0.007 to 0.05.

To provide additional modelling relevant data, the confining stress was varied at a fixed shear displacement and the fracture was subjected to shear displacement from 0.0 to 4.0 mm. Dilatational aperture as a function of confining stress at fixed displacement provides data to populate a Barton-Bandis relationship (Barton et al., 1983) for the specimen which is useful for numerically modelling flow through fracture networks (Birdsell et al., 2018). Also including the measured hydraulic aperture is useful to couple fracture porosity and permeability for modelling. In this case of the fixed displacement, hydraulic aperture parallel to the direction of shearing was 1.9 to 2.1 orders of magnitude smaller than the dilatational aperture. The dilation angle, measured from the tangent of the dilatational aperture versus total shear displacement, provides information on the linearity of the fracture deformation which in this case was quite stable at around 12°. Dilation angle is a common parameter for interface and shear failure models.

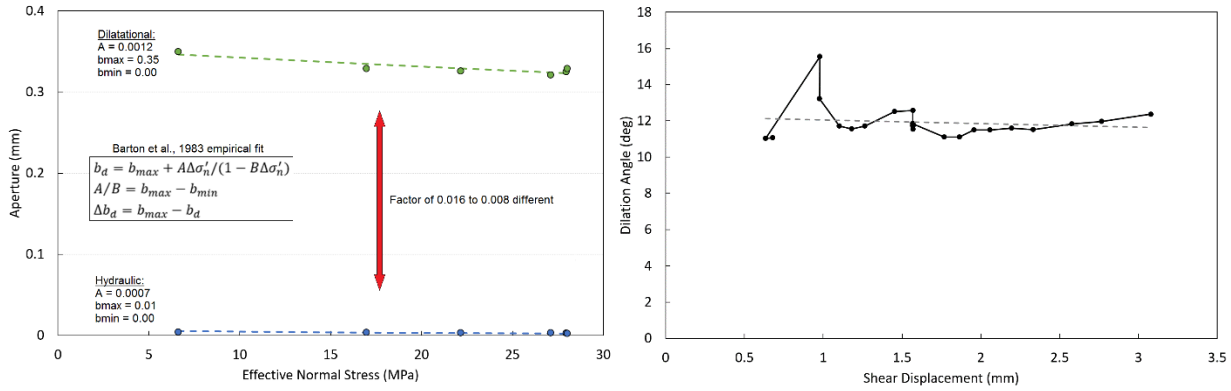

Figure 7: Results from PS01-06, the specimen containing a natural infilled foliation parallel fracture. (Left) Dilatational and hydraulic aperture with changing confining stress at fixed shear displacement. (Right) Dilation angle with increasing shear displacement.

5. CONCLUSIONS

The combination of core plug preparation, acoustic velocity testing, and triaxial direct-shear tests on the Poorman's schist from the EGS Collab E1 site have provided useful modelling parameters for this rock (Tables 1 and 2 and Figure 7). They also have helped identify that the foliation is a target for hydroshear stimulation and a key source of anisotropy in the rock's geophysical and geomechanical properties. The low initial specimen permeability at less than 0.001 mD, both for the matrix and the infilled-bonded natural fractures, combined with the high bonded shear strength indicates that hydroshearing of a bonded fracture in the E1 test bed is unlikely. However, if any pre-existing unbonded fractures are present or hydraulic fracturing injection separates the surfaces of a natural fracture, shear slip and subsequent hydroshear will be possible. The most favorable natural fractures for hydroshear stimulation are the foliation parallel fractures which tend to strike south-east with ~60° dip. Any fractures that do shear are expected to be rough with ~12° dilation angle. Subsequent formation of infilling gouge by shear slip is likely and will tend to inhibit fluid flow. Results from these experiments indicate that the injection pressure required to initiate hydroshear in the E1 test bed could be as low as 6 MPa if unbonded or weak foliation-parallel natural fractures intersect the injection zone. Injection at higher pressures increases the likelihood of hydroshearing.

ACKNOWLEDGEMENTS

The EGS Collab work in this study is supported by the U.S. Department of Energy, Office of Energy Efficiency and Renewable Energy (EERE), Geothermal Technologies Office (GTO) under Contract No. DE-AC52-06NA25396 with Los Alamos National Laboratory, led by Contract No. DEAC02-05CH11231 with Lawrence Berkeley National Laboratory. Additional support provided by Department of Energy (DOE) Basic Energy Sciences under Contract No. DE-AC52-06NA25396 is also gratefully acknowledged. We also would like to acknowledge support from E-6 at Los Alamos National Laboratory who provided the computed tomography equipment and RECON software for microtomography reconstruction. Research supporting this work took place in whole or in part at the Sanford Underground Research Facility in Lead, South Dakota. The assistance of the Sanford Underground Research Facility and its personnel in providing physical access and general logistical and technical support is gratefully acknowledged. LA-UR-19-20664.

We also wish to recognize EGS Collab Team members for providing motivation and feedback for this work: J. Ajo-Franklin, S.J. Bauer, T. Baumgartner, K. Beckers, D. Blankenship, A. Bonneville, L. Boyd, S.T. Brown, J.A. Burghardt, T. Chen, Y. Chen, K. Condon, P.J. Cook, P.F. Dobson, T. Doe, C.A. Doughty, D. Elsworth, J. Feldman, A. Foris, L.P. Frash, Z. Frone, P. Fu, K. Gao, A. Ghassemi, H. Gudmundsdottir, Y. Guglielmi, G. Guthrie, B. Haimson, A. Hawkins, J. Heise, C.G. Herrick, M. Horn, R.N. Horne, J. Horner, M. Hu, H. Huang, L. Huang, K. Im, M. Ingraham, T.C. Johnson, B. Johnston, S. Karra, K. Kim, D.K. King, T. Kneafsey, H. Knox, J. Knox, D. Kumar, K. Kutun, M. Lee, K. Li, R. Lopez, M. Maceira, N. Makedonska, C. Marone, E. Mattson, M.W. McClure, J. McLennan, T. McLing, R.J. Mellors, E. Metcalfe, J. Miskimins, J.P. Morris, S. Nakagawa, G. Neupane, G. Newman, A. Nieto, C.M. Oldenburg, W. Pan, R. Pawar, P. Petrov, B. Pietzyk, R. Podgorney, Y. Polsky, S. Porse, S. Richard, B.Q. Roberts, M. Robertson, W. Roggenthen, J. Rutqvist, D. Rynders, H. Santos-Villalobos, M. Schoenball, P. Schwering, V. Sesetty, A. Singh, M.M. Smith, H. Sone, C.E. Strickland, J. Su, C. Ulrich, N. Uzunlar, A. Vachaparampil, C.A. Valladao, W. Vandermeer, G. Vandine, D. Vardiman, V.R. Vermeul, J.L. Wagoner, H.F. Wang, J. Weers, J. White, M.D. White, P. Winterfeld, T. Wood, H. Wu, Y.S. Wu, Y. Wu, Y. Zhang, Y.Q. Zhang, J. Zhou, Q. Zhou, and M.D. Zoback.

REFERENCES

ASTM D4543-08: Standard practices for preparing rock core as cylindrical test specimens and verifying conformance to dimensional and shape tolerances. *Annual Book of ASTM Standards*, (2008). West Conshohocken, PA: ASTM International.

ASTM D5607-16: Standard test method for performing laboratory direct shear strength tests of rock specimens under constant normal force. *Annual Book of ASTM Standards*, (2016), West Conshohocken, PA: ASTM International.

Bandis, S.C., Lumsden, A.C., Barton, N.R.: Fundamentals of rock joint deformation. *Int. J. Rock Mech. Min. Sci. & Geomech. Abstr.*, 20, 249-268 (1983).

Birdsell, D.T., Rajaram, H., Karra, S.: Code development for modeling induced seismicity with flow and mechanics using a discrete fracture network and matrix formulation with evolving hydraulic diffusivity. In proceedings of the 52nd US Rock Mechanics / Geomechanics Symposium, Seattle, Washington, USA, 17–20 June (2018).

Boussinesq, J.: Mémoire sur l'influence des frottements dans les mouvements réguliers des fluids, *Journal of Mathematics Pure and Applied*, 13, 377-424 (1868).

Carey, J.W., Lei, Z., Rougier, E., Mori, H., Viswanathan, H.S.: Fracture-permeability behavior of shale. *Journal of Unconventional Oil and Gas Resources*, 11, 27-43 (2015a).

Carey, J.W., Rougier, E., Lei, Z., Viswanathan, H.: Experimental investigation of fracturing of shale with water, In proceedings of the 49th US Rock Mechanics / Geomechanics Symposium, San Francisco, CA, 28 June - 1 July (2015b).

Carey, J.W., Frash, L.P., Viswanathan, H.S.: Dynamic triaxial study of direct shear fracturing and precipitation-induced transient permeability observed by in situ x-ray radiography. In proceedings of the 50th U.S. Rock Mechanics/Geomechanics Symposium, Houston, Texas, 26-29 Jun (2016).

Detwiler, R.L., Morris, J.P.: Transmissivity anisotropy in rough-walled fractures: the combined influence of shear offset and normal deformation. In the proceedings of the 48th US Rock Mechanics / Geomechanics Symposium, Minneapolis, MN, 1-4 June (2014).

Frash, L.P., Carey, J.W., Ickes, T.: Fracturing, fluid flowing, and x-ray imaging through anhydrite at stressed conditions. In proceedings of the 52nd US Rock Mechanics / Geomechanics Symposium, Seattle, WA, 17-20 June (2018).

Frash, L.P., Carey, J.W., Ickes, T., Viswanathan, H.: Caprock integrity susceptibility to permeable fracture creation. *Journal of Greenhouse Gas Control*, 64, 60-72 (2017).

Frash, L.P., Carey, J.W., Lei, Z., Rougier, E., Ickes, T., Viswanathan, H.: High-stress triaxial direct-shear fracturing of Utica shale and in situ x-ray microtomography with permeability measurement. *Journal of Geophysical Research – Solid Earth*, 121, 5493-5508 (2016a).

Frash, L., Carey, J.W., Viswanathan, H. S., Gutierrez, M., Hampton, J., Hood, J.: Comparison of pressure, flow rate, stepped, and oscillatory control methods for fracture permeability measurements at triaxial stress conditions. In proceedings of the 50th U.S. Rock Mechanics/Geomechanics Symposium, Houston, TX, 26-29 June (2016b).

Frash, L.P., Carey, J.W., Welch, N.J.: Scalable en echelon shear-fracture aperture-roughness mechanism: theory, validation, and implications. *Journal of Geophysical Research – Solid Earth*, 124 (2019).

Frash, L.P., Gutierrez, M., Hampton, J.: Laboratory-scale-model testing of well stimulation by use of mechanical-impulse hydraulic fracturing. *SPE Journal*, 20, (2015).

Gentier, S., Lamontagne, E., Archambault, G., Riss, J.: Anisotropy of flow in a fracture undergoing shear and its relationship to the direction of shearing and injection pressure. *Int. J. Rock Mech. Min. Sci.*, 34, 3-4 (1997).

Kneafsey, T.J., Dobson, P., Blankenship, D., Morris, J., Knox, H., Schwering, P., White, M., Doe, T., Roggenthen, W., Mattson, E., Podgorney, R., Johnson, T., Ajo-Franklin, J., Valladao, C., and the EGS Collab team: An Overview of the EGS Collab Project: Field Validation of Coupled Process Modeling of Fracturing and Fluid Flow at the Sanford Underground Research Facility, Lead, SD. In proceeding of the 43rd Workshop on Geothermal Reservoir Engineering, Stanford University, Stanford, California, February 12-14, (2018).

McClure, M. and Horne, R.: Characterizing hydraulic fracturing with a tendency-for-shear stimulation test. *SPE Reservoir Evaluation and Engineering*, 17 (2014).

Oldenburg, C.M., Dobson, P.F., Wu, Y., Cook, P.J., Kneafsey, T.J., Nakagawa, S., Ulrich, C., Siler, D.L., Guglielmi, Y., Ajo-Franklin, J., Rutquist, J., Daley, T.M., Birkholzer, J.T., Wang, H.F., Lord, N.E., Haimson, B.C., Sone, H., Vigilante, P., Roggenthen, W.M., Doe, T.W., Lee, M.Y., Ingraham, M., Huang, H., Mattson, E.D., Zhou, J., Johnson, T.J, Zoback, M.D., Morris, J.P., White, J.A., Johnson, P.A., Coblentz, D.D., Heise, J.: Intermediate-Scale Hydraulic Fracturing in a Deep Mine: kISMET Project Summary (2016).

Tester, J.W., Anderson, B.J., Batchelor, A.S., Blackwell, D.D., DiPippo, R., Drake, E.M., Garnish, J.D., Livesay, B., Moore, M.C., Nochols, K., Petty, S., Toksoez, M.N., Veatch R.W.J.: *The Future of Geothermal Energy: Impact of Enhanced Geothermal Systems (EGS) on the United States in the 21st Century*, (2006). Massachusetts Institute of Technology, Idaho Falls, ID, USA, pp. 372.

Ulrich, C., Dobson, P.F., Kneafsey, T.J., Roggenthen, W.M., Uzunlar, N., Doe, T.W., Neupane, G., Podgorney, R., Schwering, P., Frash, L., Singh, A. and the EGS Collab Team: The distribution, orientation, and characteristics of natural fractures for Experiment 1 of the EGS Collab Project, Sanford Underground Research Facility. In proceedings of the 52nd US Rock Mechanics / Geomechanics Symposium, Seattle, Washington, USA, June 17–20, (2018).

Witherspoon, P.A., Wang, J.S.Y., Iwai, K., Gale, J.E.: Validity of cubic law for fluid flow in a deformable rock fracture. *Water Resources Research*, 16, 1016-1024 (1980).

Zimmerman, R.W., G.S. Bovarsson. Hydraulic conductivity of rock fractures. *Trans. Porous Media*. 23, 1-30 (1996).